



Contents lists available at ScienceDirect

Combustion and Flame

journal homepage: www.elsevier.com/locate/combustflame

Experimental study of soot and temperature field structure of laminar co-flow ethylene–air diffusion flames with nitrogen dilution at elevated pressures

H.I. Joo*, Ö.L. Gülder

University of Toronto, Institute for Aerospace Studies, 4925 Dufferin Street, Toronto, Ontario, Canada M3H 5T6

ARTICLE INFO

Article history:

Received 27 July 2010

Received in revised form 8 September 2010

Accepted 16 September 2010

Available online 8 October 2010

Keywords:

High pressure soot formation

Soot and temperature measurements

Ethylene diffusion flames

Soot yield at high pressure

ABSTRACT

An experimental study has been conducted to investigate soot formation in laminar co-flow ethylene–air diffusion flames with nitrogen dilution from a co-flow circular nozzle at pressures from 10 to 35 atm. Spectral soot emission (SSE) diagnostic technique was used to determine the radially resolved soot and temperature field structure. Constancy of ethylene and nitrogen flow rates were maintained and the flow rates of ethylene and nitrogen were selected such that no smoke was emitted even at the highest soot loadings. The flame height, marked by visible flame radiation, remained constant at about 5.5 mm and the cross-sectional area of the flame decreased with increasing pressure. At 10 atm, the peak soot concentration of less than 8 ppm, was measured near the flame tip. At 35 atm, the peak soot concentration of about 62 ppm, was measured near the mid-height of the flame. The conversion of carbon in the fuel to soot was strongly dependent on pressure particularly in the lower pressure range. At higher pressure this dependence was weaker. The peak carbon conversion to soot, 6.5%, was observed at 30 atm and remained constant to 35 atm. Temperatures increased along the flame axis and the peak temperature was observed near the flame tip to indicate complete soot oxidation.

© 2010 The Combustion Institute. Published by Elsevier Inc. All rights reserved.

1. Introduction

The bulk majority of transport vehicles we use today rely on the combustion of hydrocarbon fuels to provide power. However, due to the carbon-based nature of the fuel source, combustion of the hydrocarbon fuel emits solid carbon particulate matter in the form of visible smoke or soot, if these carbonaceous matter is not oxidized fully in the flame. The formation of soot has important consequences because soot particles not only pollute the environment, but pose adverse health effects to people as well. These soot particles have carcinogenic properties and yield ill-effects on human lungs [1–3]. Furthermore, soot particles have been implicated as a major contributor to climate forcing. The soot particles from aircraft engine exhaust may be one of the leading culprits of global warming, perhaps second only to that of CO₂ [4]. The soot particles affect the earth's temperature and climate, both regionally and globally by altering the radiative properties of the atmosphere. The deposition of soot aerosol in snow and ice alters its reflectivity (snow albedo) and thus the ability to reflect the incident sunlight is reduced [4]. This introduces another warming effect and the effect of snow albedo may be responsible for a quarter of global warming that has been observed [5].

Soot formation and oxidation during the combustion process is dependent on several parameters. One of the most important of

these is the pressure which causes a significant increase in soot production with increasing pressure. Since practical work producing combustion devices, such as internal combustion engines and gas turbines operate at elevated pressures, a close examination of soot formation and oxidation in the high pressure environment is required to address the environmental problems posed by these devices. Efforts to elucidate the effect of pressure on soot formation have been focused largely on providing a functional relationship between pressure and soot formation. However, only a few experimental studies have been conducted at high pressures [6–11]. These studies report a significant increase in soot concentration measurements with increasing pressure. Flower and Bowman [7] and Lee and Na [9] employed a laser diagnostic technique to study axisymmetric laminar diffusion flames of ethylene at elevated pressures. Flower and Bowman [7] report that the maximum integrated soot volume fraction across the flame diameter scales with pressure raised to a power of 1.2 for pressures between 1 and 10 atm, while measurements of Lee and Na [9] indicate a similar pressure scaling with the exponent 1.26 for pressures up to 4 atm. McCrain and Roberts [10] measured path-integrated soot volume fraction (across the flame diameter) in methane (1–25 atm) and ethylene (1–16 atm) flames and report the pressure exponents as 1.0 and 1.2, respectively. To our knowledge, measurements with ethylene diffusion flames at elevated pressure that are available in the literature are up to 16 atm [10]. Experimental work by Thomson et al. [11] also measured path-integrated soot volume fraction up to 40 atm and similar pressure exponents

* Corresponding author. Fax: +1 416 667 7799.

E-mail address: h.joo@utoronto.ca (H.I. Joo).

to those reported in [7,9,10] have been found. In high pressure laminar diffusion flames, however, fraction of carbon in the fuel that is converted to soot, rather than the line-of-sight integrated soot volume fraction, is a better measure to assess the sensitivity of soot formation to pressure [7,11]. Measurements by Thomson et al. [11] with methane flames report unity pressure exponent for the percentage of fuel's carbon converted to soot for pressures between 5 and 20 atm, and 0.1 for pressures between 20 and 40 atm. Similarly, measurements by Bento et al. [6] on laminar diffusion flames of propane report the scaling pressure exponent as 3.3 from atmospheric to 2 atm, and 1.1 for pressures between 2 and 7.2 atm. In more recent findings, work by Joo and Gülder [8] on high pressure methane laminar diffusion flames report the pressure exponent as 0.73 for pressures between 10 and 30 atm, and 0.33 for pressures between 30 and 60 atm.

It is important to recognize that the pressure sensitivity of the fraction of carbon in the fuel converted to soot from C_1 and C_3 hydrocarbons appeared to decrease with pressures approaching the critical pressure of the fuel in the experimental studies presented in [6,8,11]. Considering the difficulties involved in conducting high pressure experiments and the importance of such fuels as ethylene as a key intermediate in the combustion process, additional measurements are required to provide support to the accuracy of recent experimental data in [6,8,11] and to the development of a robust model. Thus, the main objective of this study is to investigate the pressure sensitivity of soot formation in nitrogen-diluted ethylene–air diffusion flames by providing radially resolved soot concentration and temperature measurements at elevated pressures. The information provided here covers a substantial pressure range and offers detailed measurements pertaining to ethylene up to 35 atm.

2. Experimental methodology

Experiments are conducted in the high pressure combustion chamber with a design pressure of 110 atm that is equipped with three quartz glass windows located at 0° , 90° and 180° for a line-of-sight and 90° scattering and imaging measurements. The schematic drawing of the chamber is provided in Fig. 1 and described in [6,8]. The annular co-flow burner is comprised of a straight bored-through stainless steel fuel nozzle with an exit diameter of 3 mm and an air nozzle diameter of 25.4 mm. The fuel nozzle is tapered towards the tip to form a knife-edge at the rim. Sintered metal foam elements are included in the fuel and air nozzles to straighten and reduce the instabilities in the flow and to create a

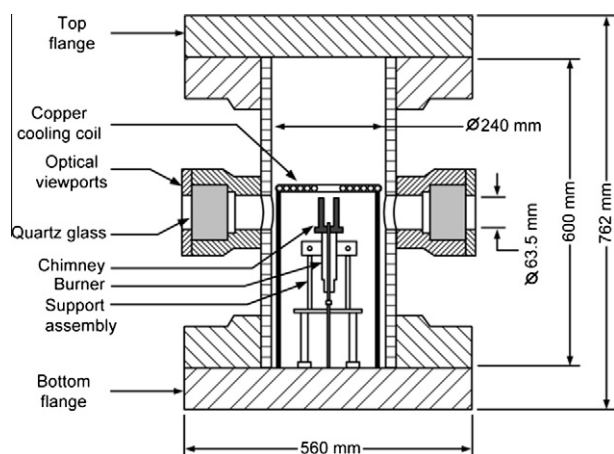


Fig. 1. Schematic drawing of the high pressure combustion chamber with the overall dimensions.

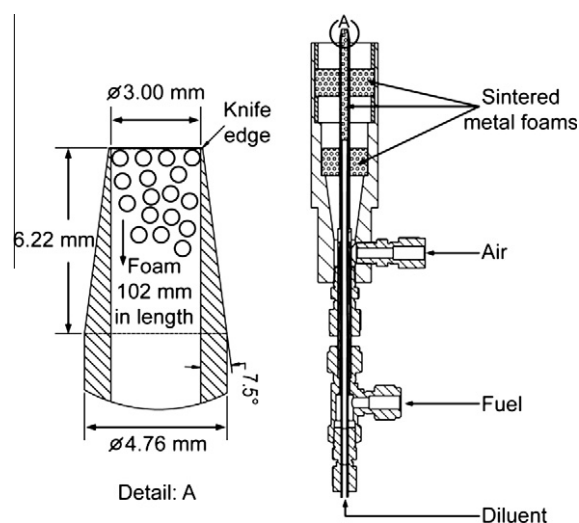


Fig. 2. Schematic drawing of the burner.

top hat exit velocity profile as the gases leave the foam elements. The schematic drawing of the burner is provided in Fig. 2.

Ethylene and nitrogen were introduced to the burner directly and mixed in the fuel tube prior to leaving the foam element. Constant ethylene mass flow rate of 0.27 mg/s that corresponds to carbon mass flow rate of 0.232 mg/s was maintained at all pressures. Constant nitrogen mass flow rate of 1.35 mg/s was maintained at all pressures, that is, nitrogen was added to the ethylene fuel stream at the ratio of 5–1 by volume. Air co-flow rate was fixed at 0.4 g/s for soot and temperature measurements at elevated pressures. These flow rates were selected to produce a non-smoking flame at 35 atm and yet, yield sufficient soot radiation emission without saturating the field.

The theory of the spectral soot emission diagnostic (SSE) are described previously in [6,11,12], and the detailed layout of the experimental setup are described in [8]. In SSE, line-of-sight radiation emission from soot is measured along chords through the flame. A series of emission projections at a given axial location in the flame can be inverted to obtain radially resolved emission rates from which temperature and soot volume fraction can be determined when soot optical properties are known [13]. Soot radiation emission measurements are recorded every 50 μm from left- to right-side of the flame to scan the entire cross-section at axial height location. The measurements are repeated along the axial height locations in the flame at increments of 0.5 mm until the entire flame is scanned.

3. Results and discussions

3.1. Physical flame appearance

At atmospheric conditions, the flame was completely blue¹ with no visible sooting zone. The flame attained a saucer shape and hovered at about two tube diameters away from the fuel nozzle tip, Fig. 3. The flame was very sensitive to the slightest flow instabilities. Any disturbances in the flow field resulted in a sudden flame blow-off. As the pressure increased, however, the flame became stable and the lift-off height decreased. A yellow sooting region appeared near the tip of the flame and increasingly filled the portion occupied previously by the blue flame. At 10 atm and above, the flame was attached by the typical blue flame zone near the fuel nozzle rim,

¹ For interpretation of color in Figs. 3 and 4, the reader is referred to the web version of this article.

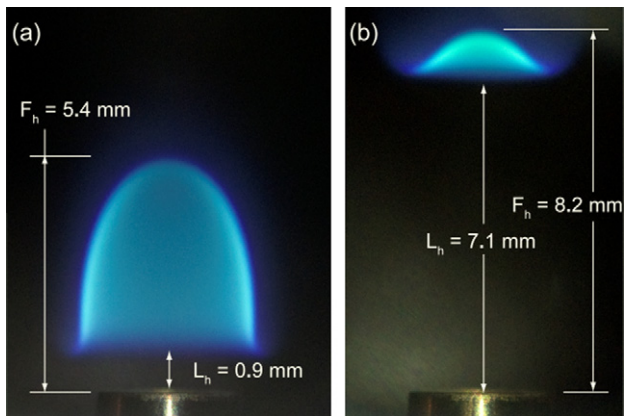


Fig. 3. Images of nitrogen-diluted laminar ethylene-air diffusion flames at atmospheric conditions. Ethylene flow rate is 0.27 mg/s and nitrogen flow rate is 1.35 mg/s. (a) Air co-flow rate 0.2 g/s, (b) air co-flow rate 0.28 g/s.

Fig. 4, and showed no sensitivity towards ambient aerodynamic forces. At 35 atm, only a small portion of the flame very close to the fuel nozzle rim remained blue, Fig. 4. The visible flame heights in this work remained constant at about 5.5 mm for pressures between 10 and 35 atm. The physical appearance of the flame presented in this work is consistent with the theory [14,15] and the work presented in [6,8,11].

As the pressure increased, axial flame diameter decreased to give an overall stretched appearance to the flame as noted by previous investigators [6–8,11]. For pressures between 10 and 35 atm, the cross-sectional area of the flame decreased as $A_c \propto P^{-1}$ to give a pinched appearance to the flame, Fig. 4. This observation is in agreement with the previous experimental studies [6,8,10,11] as well as to the recent numerical effort in [16] that showed that the axial velocity profiles are independent of pressure along the flame centerline in methane diffusion flames between 0.5 and 4 MPa. The inverse dependence of the flame cross-sectional area to pressure implies that the residence times are independent of pressure and thus the measurements can be compared at the same height above the burner exit [6,8,11].

The constancy of the residence time can be illustrated by using the flame height expression developed in [14]. To a first approximation, the height of the buoyancy-dominated laminar co-flow diffusion flame established on a circular-port burner under fixed fuel flow rate, scales with the volumetric fuel flow rate Q , and molecular diffusivity, D as,

$$H \propto \frac{Q}{D} \propto \frac{\nu A}{D} \quad (1)$$

where ν is the fuel exit velocity and A is the nozzle exit area [6]. For a fixed mass flow rate, density scales with pressure and thus the velocity varies inversely with pressure. However, since the molecu-

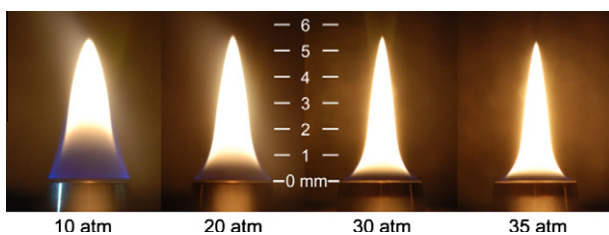


Fig. 4. Images of nitrogen-diluted laminar ethylene-air diffusion flames at pressures 10–35 atm. The visible flame height remained constant at about 5.5 mm. Ethylene flow rate is 0.27 mg/s and nitrogen flow rate is 1.35 mg/s. Co-flow air is fixed at 0.4 g/s.

lar diffusivity, D , is inversely proportional to pressure, the height of the diffusion flame is independent of pressure. Hence, the average velocity within the flame envelope will not change with pressure if the flame cross-sectional area varies inversely with pressure. That is, as the pressure increases, the material flow within the flame envelope will be through a narrower cross-section but at a higher density, thus keeping the average velocity constant at a given height.

3.2. Soot concentration measurements

A three-dimensional representation of radial soot volume fraction profiles for the ethylene-air laminar diffusion flames diluted with nitrogen as a function of pressure from 10 to 35 atm is presented in Fig. 5. Detailed measurements of soot concentration profiles are provided in Fig. 6. Overall, the pressure has a significant effect on sooting ethylene-air diffusion flames. The measured maximum soot concentration increased from less than 8 ppm at 10 atm to over 62 ppm at 35 atm. Soot forms first in an annular band near the burner rim. With increasing pressure, the annular band becomes less pronounced at higher axial flame locations, and the maximum soot concentration is observed near the flame centerline, Fig. 6. The contraction of the flame diameter with pressure is reflected by the decreasing radial distances of the peaks in the radial soot volume fraction profiles for pressures between 10 and 35 atm, Fig. 6. The axial location of the maximum soot concentration decreased from 4.5 mm at 10 atm to 3.5 mm at 35 atm. The decrease in the axial location is reflective of the fact that the sooting region expands towards the burner rim with increasing pressure.

As expected, soot concentrations are relatively low because nitrogen was added to the ethylene fuel stream. Using an additive has three general effects as described extensively by Du et al. [17] and Liu et al. [18]: (1) thermal effect due to the change in the flame temperature; (2) direct chemical effect due to the active participation of the diluent in the chemical reaction concerning soot formation and oxidation and (3) dilution effect since the concentrations of the reactive species responsible for soot formation is reduced. However, it is difficult to isolate properly the individual effects because these effects are intimately coupled. For example, it is argued

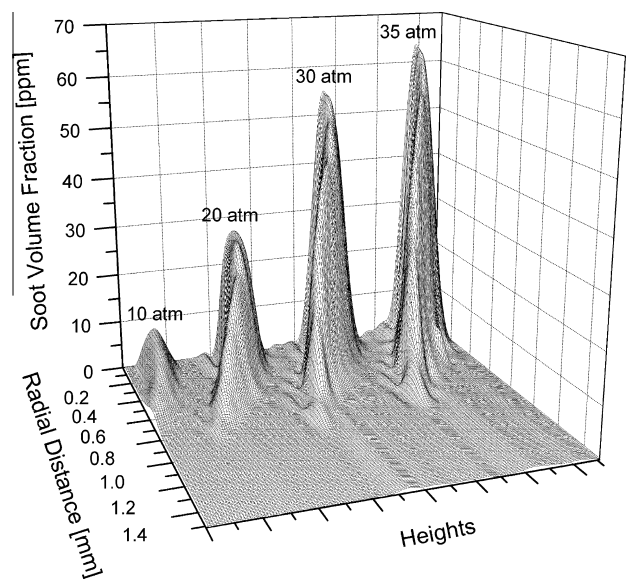


Fig. 5. A three-dimensional representation of soot concentration profiles. The “Heights” on the figure axis represents successive axial flame locations along the flame used in the measurements for each flame at various pressures indicated.

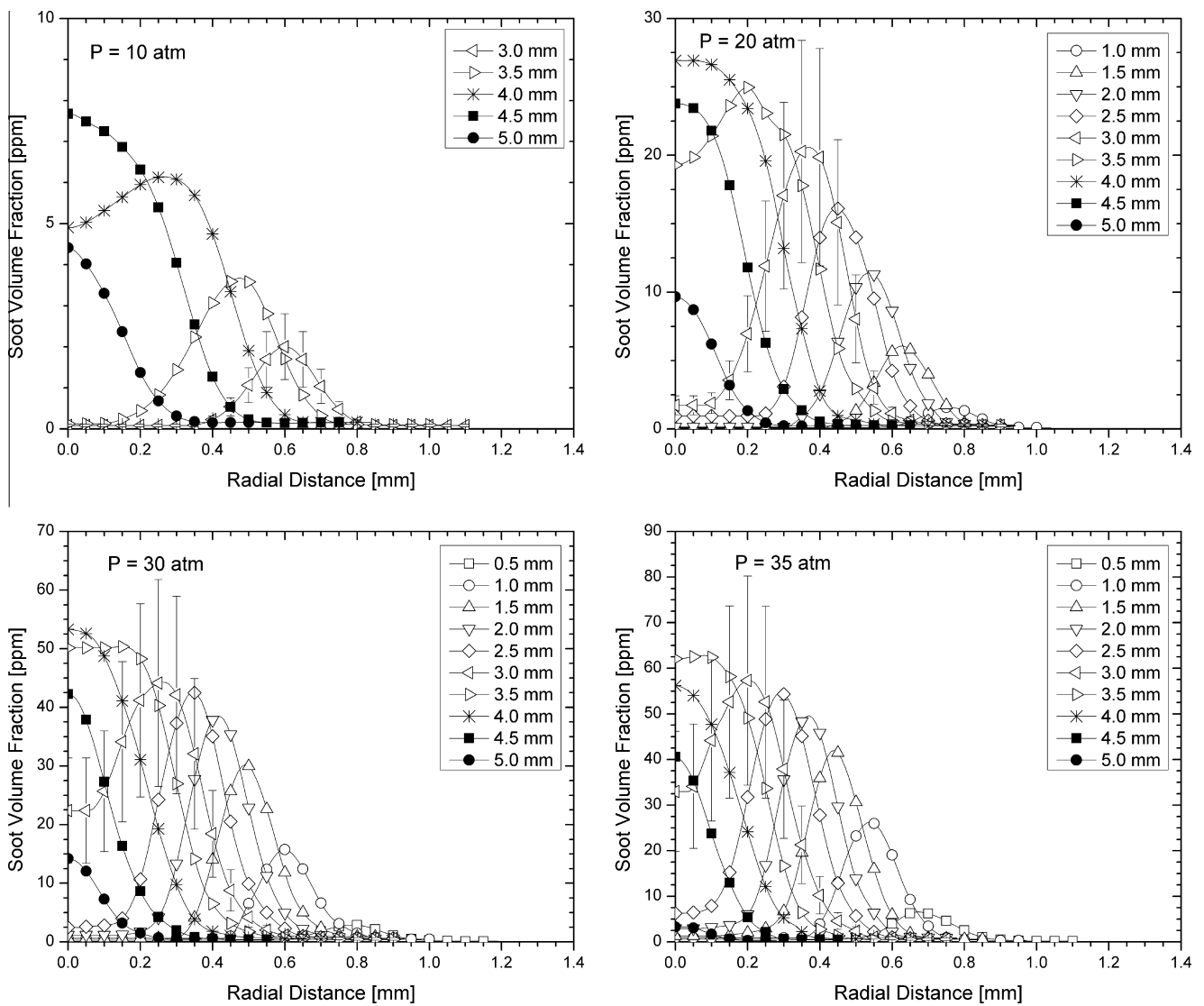


Fig. 6. Radially resolved soot concentration profiles at pressures 10–35 atm.

that an additive reduces the flame temperature (thermal effect) by lowering the concentration of the species that are responsible for the exothermic reaction (dilution effect). Furthermore, the additive itself can participate directly in the chemical reaction to alter the flame temperature and the mechanisms responsible for the soot formation and oxidation. Although some of the heat that is liberated from the reaction is absorbed by nitrogen, active participation of nitrogen in the reaction to have a major chemical influence is not considered substantive. In view of the thermal consideration, there is an obvious thermal effect in the present ethylene–air experiments because the calculated flame temperature with the addition of nitrogen to the fuel stream is about 310 K lower than pure ethylene–air flame temperature. It is believed that lower temperatures inhibited pyrolysis reaction rates and thereby reduced the concentrations of the precursor species responsible for soot formation.

As suggested by previous investigators [7,11], the sooting propensity of the flame to pressure is assessed better by determining the percentage of total carbon in the fuel converted to soot, rather than path-integrated soot volume fraction. The same approach is adopted here to assess the influence of pressure. The mass flow rate of carbon in the form of soot, \dot{m}_s , can be determined through the relationship,

$$\dot{m}_s(z) = v_z(z)\rho_s \int 2\pi r f_v(r, z) dr \quad (2)$$

where v_z is the axial velocity, $\rho_s = 1.8 \text{ g/cm}^3$ is the soot density and z is the axial height. The axial velocity is estimated as $v_z(z) = (2az)^{1/2}$, where a is an acceleration constant commonly assumed to be 25 m/s^2 [7,15]. The percentage of carbon in the fuel converted to soot is then simply $\eta_s = \dot{m}_s/\dot{m}_c$ where \dot{m}_c is the carbon mass flow rate at the nozzle exit. It should be noted that Eq. (2) assumes that the axial velocity is uniform within the flame envelope. Although this is not entirely correct, especially lower in the flame and near the burner tip, at higher axial locations it is a sound approximation that has been used in previous studies [6–8,11] and it was one of the main assumptions in Roper's formulation [14]. The uncertainty introduced by this assumption in the maximum carbon conversion to soot is estimated to be less than 15%, in view of the velocity field calculations in similar flames [16]. The maximum percentage of carbon conversion to soot, observed at 30 atm at 3 mm axial flame location, is about 6.5%, Fig. 7. At lower pressures, the peak conversion occurs closer to the flame tip at about 4 mm flame height. In general, the flame height at which maximum fuel carbon conversion occur decreases with increasing pressure. This is due to the fact that sooting zone expanded towards the nozzle with increasing

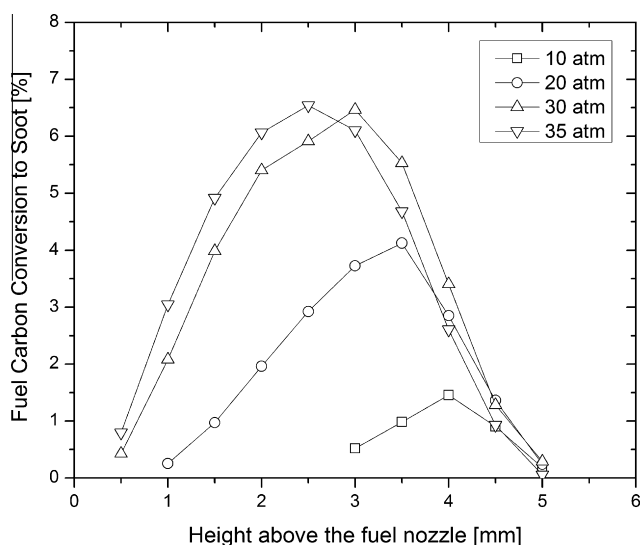


Fig. 7. Percentage of carbon in the fuel converted to soot along the flame axis.

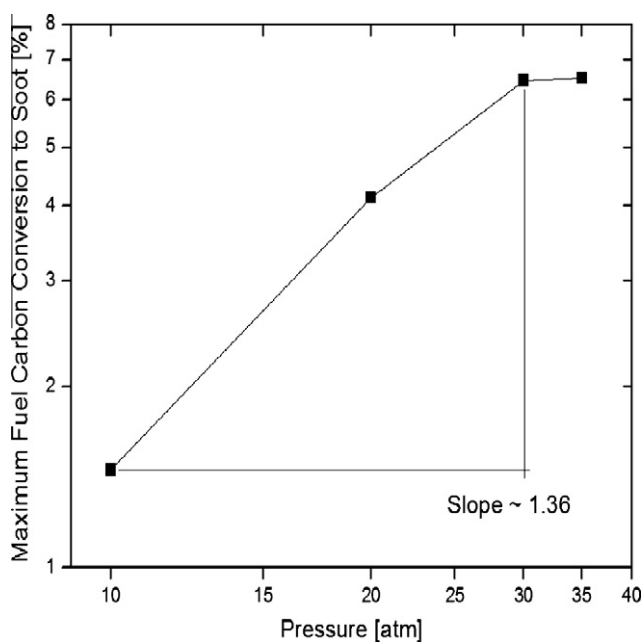


Fig. 8. Maximum conversion of carbon in the fuel to soot at pressures 10–35 atm.

pressure and thus the peak conversion occurs at approximately mid-height of the flame at higher pressures. A logarithmic plot of maximum percentage conversion of carbon to soot as a function of pressure is shown in Fig. 8. The percentage of fuel carbon conversion to soot has a power-law relationship of $\eta_s \propto P^n$ where n is about 1.36 for pressures 10–30 atm. The pressure exponent for the power-law relationship reported in this work is in agreement within experimental error margins with the exponents reported in Thomson et al. [11] and Joo and Gülder [8] for the similar pressure range in methane diffusion flames.

The fuel carbon conversion to soot appears to have peaked at pressures approaching the critical pressure of the fuel, Fig. 9. In Fig. 9, the abscissa represents reduced pressure, defined here by normalizing the actual pressure by the respective average critical pressure of the fuel and oxidizer mixture of stoichiometric proportions since the critical pressures of each of the gases are relatively

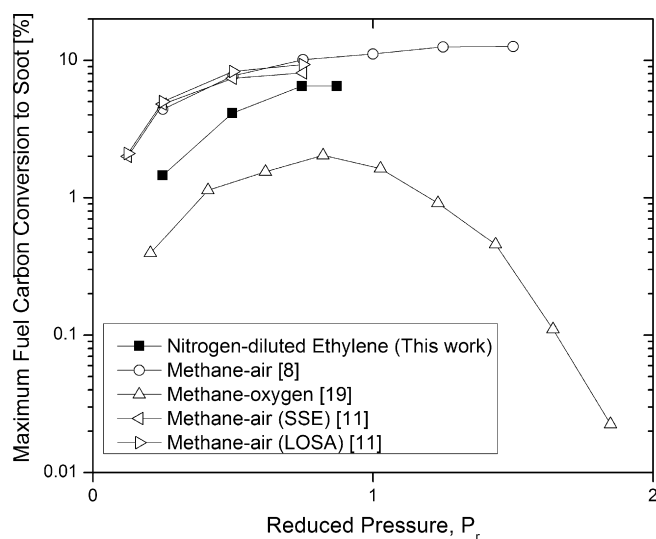


Fig. 9. Maximum conversion of carbon in the fuel to soot as a function of reduced pressures normalized by average critical pressures of the fuel-oxidizer stoichiometric mixture.

Table 1
Critical properties of the gases [20].

Gas	Molar mass (g/mol)	Critical pressure atm (MPa)	Critical temperature (K)
Methane	16.04	45.8 (4.64)	190.8
Oxygen	32.00	50.2 (5.09)	154.6
Nitrogen	28.01	33.6 (3.40)	126.3
Ethylene	28.05	49.7 (5.04)	282.4

similar. The critical properties of the gases are tabulated in Table 1. In all of the experiments, the plot reveals a declining sensitivity to pressure as it approaches the reduced pressure of unity with the exception of methane–oxygen case. In the methane–oxygen case, there is a reduction in the fuel carbon conversion to soot at reduced pressure $P_r = 1$. This confirms the previous experimental findings in [6,8,11] where they also report a declining pressure dependence of the fraction of fuel carbon converted to soot at pressures approaching the critical pressure of the fuel. It is possible that at higher pressures, the fuel carbon conversion to soot will perhaps exhibit a decreasing trend to a negligible quantity as shown by methane–oxygen flames in [19]. In [19], the percentage of conversion of carbon in the fuel to soot initially increases with pressure up to 40 atm then decreases to less than one-tenth of a percent when the pressure is increased further to 90 atm. A possible reason could be that at elevated pressure, oxygen is entrained strongly into the fuel stream near the burner tip and thus, the soot inception and growth are inhibited early in the lower portion of the flame [16].

3.3. Temperature measurements

The soot temperature profiles for the ethylene–air flames are similar to those reported in [8] for methane–air flames. Detailed measurements of temperature profiles are provided in Fig. 10. Generally, the temperatures increased along the flame axis and the peak temperature was observed near the flame tip to confirm the non-smoking nature of the flame by completely oxidizing the soot within the flame envelope. In general, temperatures decrease with increasing pressure due to increased soot radiation emission with rising pressure. The decrease in temperature, however, is small and it is comparable to [8] with similar soot loadings.

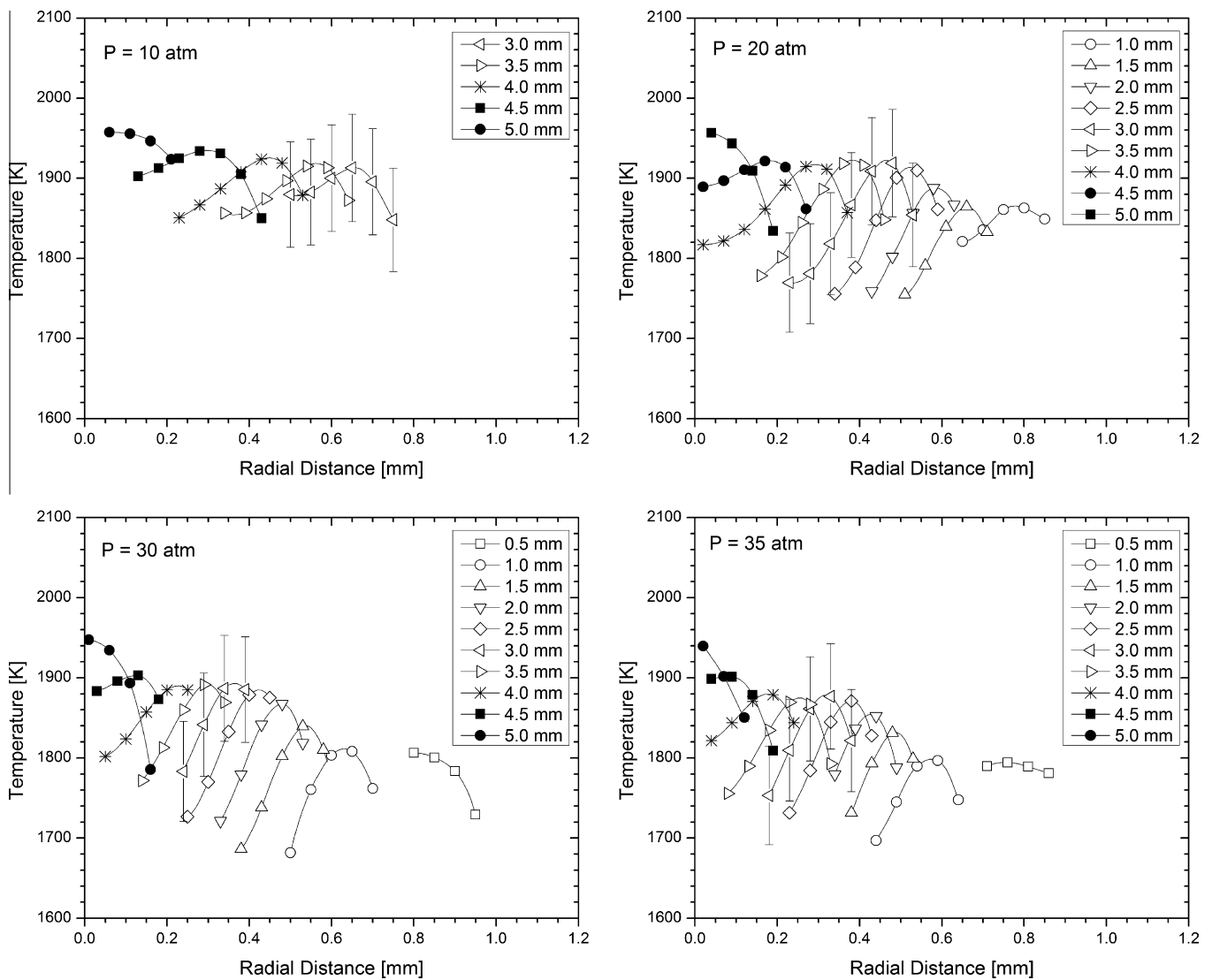


Fig. 10. Radially resolved temperature profiles at pressures 10–35 atm.

The value of the refractive index is required to calculate the soot volume fraction and temperatures from the emission data. However, there is a lack of understanding of the dependence of soot optical properties, specifically soot refractive index on temperature, wavelength, and soot aggregate size. The implications of this uncertainty are discussed in detail in [6] and the errors introduced in temperature and soot concentration measurements are summarized. To be consistent with our previous measurements of soot and temperature by the soot emission spectroscopy [6,8,11,12,19], we used the same value for the soot refractive index in the current work. Since the spectral soot emission diagnostic used in this study measures the soot radiation emission to determine the soot temperature and soot volume fraction, measurements can be only made in locations where sufficient soot exists to provide a resolvable signal. These regions typically occur at radial locations near the peak soot concentrations where they provide the best signal to calculate the temperatures. Temperatures can be inaccurate in the flame core due to low soot concentrations relative to the peak concentrations in the flame annulus [11]. Furthermore, previous characterization of SSE diagnostic [12] has shown that temperature at the edge of the flame annuli are lower than the temperature predicted by flame models or other experi-

mental diagnostics. It is believed that the inversion algorithm used to invert the rapidly decreasing line-of-sight emission intensities at the flame edge introduces errors to create this temperature difference. Thus the peak temperatures in the reaction zone are under-predicted. It is possible that the limitations of the temperature measurements in the core and on the outside of the soot annulus may be caused by beam steering when the SSE diagnostic is applied to a flame with such intense temperature gradients. Therefore, the radial temperature profiles provided in Fig. 10 are limited to the annuli regions where sufficient soot exist to provide a resolvable signal.

The soot particles in the flame absorb and emit radiation, thus emissions from soot are inherently attenuated by other soot particles along the detection path in the flame. However, the cross-sectional area of the flame decreased with pressure so the length at which the emissions are attenuated is shortened. Since the attenuation of emission is a function of the product of the soot concentration and the absorption path length, attenuation by soot particles in the flame is assumed negligible. Furthermore, the flame emission model presented in [12] showed that attenuation of emission by soot particles introduced only a small error into the measurements (i.e., <2%). Thus, no attenuation correction is applied to the

data even for the highest soot loadings observed in the study. The total uncertainties in the temperature and soot volume fraction measurements were estimated as 3.5% and 40%, respectively, with 95% confidence interval.

4. Concluding remarks

In the present investigation, the influence of pressure on soot formation was examined and measurements of soot concentration and temperature field structure were presented. At atmospheric conditions, the flame was lifted and not stable at high air co-flow rates. For pressures between 10 and 35 atm, the flame height, marked by visible soot radiation, remained constant at about 5.5 mm and the cross-sectional area of the flame decreased with pressure. There was almost an eightfold increase in the measured soot volume fraction when the pressure was increased from 10 to 35 atm. The percentage of fuel's carbon content conversion to soot was strongly dependent on pressure. At 30 atm and above, however, the pressure dependence got weaker and at 35 atm, the percentage of carbon in the fuel converted to soot appeared to become independent of pressure. The maximum percentage of carbon in the fuel converted to soot, 6.5%, was observed at 30 atm and remained constant to 35 atm. Our results are consistent with the previous observations in other gaseous fuels that pressure sensitivity of conversion of fuel's carbon to soot decreases with pressures approaching the critical pressure of the fuel. Generally, the temperatures increased along the flame axis and decreased with pressure. The peak temperature was observed near the flame tip to indicate complete soot oxidation.

Acknowledgments

We acknowledge an infrastructure grant provided by Canadian Foundation for Innovation (CFI) for building the high-pressure combustion vessel and associated components as well as acquiring the diagnostic equipment. Operational funds for this work have been provided by Natural Sciences and Engineering Research Council (NSERC), and Canadian Space Agency (CSA).

References

- [1] H.J. Bunn, D. Dinsdale, T. Smith, J. Grigg, *Thorax* 56 (2001) 932–934.
- [2] F. Horak Jr., M. Studnicka, C. Gartner, J.D. Spengler, E. Tauber, R. Urbanek, A. Veiter, T. Frischer, *Eur. Respir. J.* 19 (2002) 838–845.
- [3] N. Kulkarni, N. Pierse, L. Rushton, J. Grigg, *N. Engl. J. Med.* 355 (2006) 21–30.
- [4] M.Z. Jacobson, *Nature* 409 (2001) 695–697.
- [5] J. Hansen, L. Nazarenko, *Proc. Natl. Acad. Sci. USA* 101 (2004) 423–428.
- [6] D.S. Bento, K.A. Thomson, Ö.L. Gülder, *Combust. Flame* 145 (2006) 765–778.
- [7] W.L. Flower, C.T. Bowman, *Proc. Combust. Inst.* 21 (1986) 1115–1124.
- [8] H.I. Joo, Ö.L. Gülder, *Proc. Combust. Inst.* 32 (2009) 769–775.
- [9] W. Lee, Y.D. Na, *JSME Int. J. Ser. B* 43 (2000) 550–555.
- [10] L.L. McCrain, W.L. Roberts, *Combust. Flame* 140 (2005) 60–69.
- [11] K.A. Thomson, Ö.L. Gülder, E.J. Weckman, R.A. Fraser, G.J. Smallwood, D.R. Snelling, *Combust. Flame* 140 (2005) 222–232.
- [12] D.R. Snelling, K.A. Thomson, G.J. Smallwood, Ö.L. Gülder, E.J. Weckman, R.A. Fraser, *AIAA J.* 40 (2002) 1789–1795.
- [13] C.J. Dasch, *Appl. Opt.* 31 (1992) 1146–1152.
- [14] F.G. Roper, C. Smith, A.C. Cunningham, *Combust. Flame* 29 (1977) 227–234.
- [15] F.G. Roper, *Combust. Flame* 29 (1977) 219–226.
- [16] F. Liu, K.A. Thomson, H. Guo, G.J. Smallwood, *Combust. Flame* 146 (2006) 456–471.
- [17] D.X. Du, R.L. Axelbaum, C.K. Law, *Proc. Combust. Inst.* 23 (1990) 1501–1507.
- [18] F. Liu, H. Guo, G.J. Smallwood, Ö.L. Gülder, *Combust. Flame* 125 (2001) 778–787.
- [19] H.I. Joo, Ö.L. Gülder, *Combust. Flame* 157 (2010) 1194–1201.
- [20] N.B. Vargaftik, Y.K. Vinogradov, V.S. Yargin, *Handbook of Physical Properties of Liquids and Gases*, third ed., Begell House, Inc., 1996.